Macromolecules

Article

pubs.acs.org/Macromolecules

Exploring the Volume Phase Transition Behavior of POEGA- and PNIPAM-Based Core–Shell Nanogels from Infrared-Spectral Insights

Lei Hou,[†] Kai Ma,[‡] Zesheng An,[§,*] and Peiyi Wu[†,*]

[†]State Key Laboratory of Molecular Engineering of Polymers, Department of Macromolecular Science, and Laboratory of Advanced Materials, Fudan University, Shanghai, 200433, China

[‡]Department of Chemistry, Shanghai University, Shanghai 200444, China

[§]Institute of Nanochemistry and Nanobiology, College of Environmental and Chemical Engineering, Shanghai University, Shanghai, 200444, China

Supporting Information

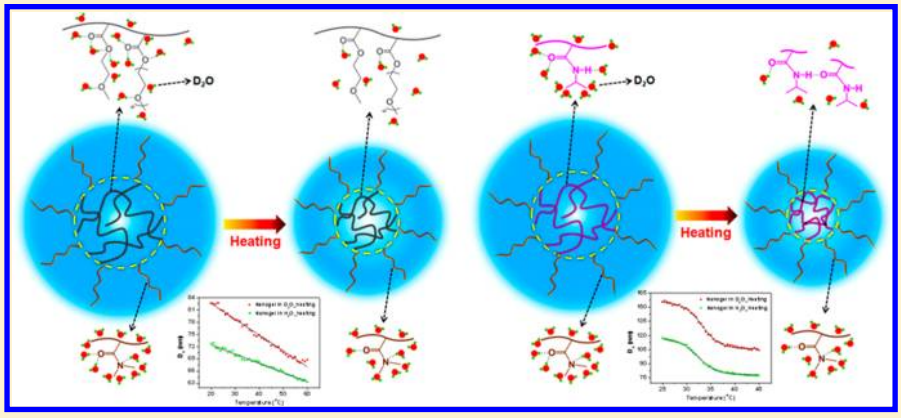

ABSTRACT: The volume phase transition behavior of well-defined thermally responsive poly(2-methoxyethyl acrylate-*co*-poly(ethylene glycol) methyl ether acrylate)/poly(*N*,*N*′-dimethylacrylamide) (P(MEA-*co*-PEGA)/PDMA) and poly(*N*-isopropylacrylamide)/poly(*N*,*N*′-dimethylacrylamide) (PNIPAM/PDMA) core–shell nanogels, synthesized via reversible addition–fragmentation chain transfer (RAFT) mediated aqueous dispersion polymerization, is studied and compared by applying FTIR measurements in combination with two-dimensional correlation spectroscopy (2Dcos). Analysis through spectral insights clearly illustrates that the continuous dehydration of the C═O groups in the P(MEA-*co*-PEGA)/PDMA nanogel core predominates the linear volume phase transition while the hydrogen bonding transformation in the PNIPAM/PDMA nanogel core leads to the abrupt decrease in nanogel size on heating. Additionally, considering the core and the shell separately, the data shows that, for both nanogels, the inner core contributes much more to the volume phase transition and the outer shell only undergoes slight dehydration following the core on heating.

1. INTRODUCTION

Nanogels, or microgels, being able to swell in a good solvent, are cross-linked polymeric particles in the colloidal range.[1−3] When focusing on these polymer-based three-dimensional networks in the submicrometer size range, stimuli responsive nanogels have attracted much attention. In addition to tunable chemical functionality, high solvent content and good biocompatibility, stimuli responsive nanogels can change their swelling behavior in response to external stimuli, such as temperature, pH, pressure, and ionic strength. Compared with macroscopic gels, nanogels show rather faster response to vary their volume upon external stimuli due to their smaller size, which makes them attractive candidates for plenty of potential applications in drug delivery,[4,5] chemical separation,[6] catalysts,[7,8] photonics,[9] imaging,[10,11] sensing,[12,13] and nanoreactors,[14] to name but a few.

The most frequently studied responsive building block for nanogels is poly(*N*-isopropylacrylamide) (PNIPAM),[2,15] a famous temperature-sensitive polymer that exhibits an abrupt coil-to-globule phase transition when the temperature goes above its lower critical solution temperature (LCST, ∼33 °C). In other words, PNIPAM-based nanogels swell at low temperatures while collapse at high ones because of the increase in hydrophobicity of the polymer chains upon heating. More recently, a new family of polymers based on oligo(ethylene glycol) (meth)acrylate(OEG(M)A) have been developed to display thermally responsive properties.[16−18] In analogy to PNIPAM, the LCST-type behavior of OEG(M)A copolymers is relatively insensitive to ionic strength, chain

Received: October 23, 2013
Revised: January 3, 2014
Published: January 23, 2014

length, concentration and pH.[19] Besides, OEG(M)A copolymers show more fascinating features including good biocompatibility, tunable LCST, antifouling properties at temperatures below their LCST, and complete reversibility of thermal transition, which is free of broad hysteresis.[20−23] Owing to the above-mentioned characteristics, OEG(M)A copolymers have become the rising stars in diverse materials arenas and been widely investigated throughout this field, including the preparation of nanogels.[24−28]

In order to investigate the morphologies, compositions and volume transitions of nanogels, a series of techniques have been developed, including experimental methods such as scanning electron microscopy (SEM), transmission electron microscopy (TEM), light scattering,[29,30] neutron scattering,[31−33] nuclear magnetic resonance (NMR),[34,35] and some theoretical modellings.[36] As is well-known, hydrogen bond plays a vital part in the delicate balance between hydrophobic and hydrophilic interactions in nanogels. The polymer−solvent hydrogen bonds dominate below the volume phase transition temperature (VPTT), resulting in solvated polymers and well swollen nanogels. Upon heating, the hydrogen bonds between polymers and solvent gradually break; above the VPTT, hydrophobic interactions in the polymeric chains are dominant, then the nanogels collapse. It is widely believed that the Fourier transform infrared spectroscopy (FTIR) is a suitable method to explore such hydrophilic/hydrophobic interactions in nanogels. Richtering and co-workers[37] utilized temperature-dependent FTIR to explore microgels built from NIPAM and *N*,*N*-diethylacrylamide (DEAAM) with different architectures, namely core−shell and random copolymers, and correlated the inter- and intramolecular hydrogen bonds with the microgel architecture. They discovered that the unusual synergisitic depression of VPTT of the copolymer microgels was originated from strong hydrogen bonds between neighboring NIPAM and DEAAM groups. Later, the same group investigated the influence of monomer substitution pattern of different copolymers on the phase transition behavior with two different copolymer microgel series: PDEAAM and PNIPAM or PDEAAM and poly(*N*-isopropyl methacrylamide) (PNIPMAM), by means of temperature-resolved FTIR.[38] They revealed that the additional α-methyl group of the PNIPMAM backbone would restrain the flexibility of the entire nanogel system and hence inhibit the formation of intramolecular hydrogen bonds, which leads to the VPTT of PNIPMAM-based microgels being higher than that of the PNIPAM systems. Recently, Maeda et al.[39] investigated the hydration of P(*N*-vinyl carprolactam) (PVCL) microgels, another intensively studied thermally responsive microgel system, by mid-infrared (MIR) and near-infrared (NIR) spectroscopy. They demonstrated that the C−H bands and C−N band underwent red shifts while blue shifts occurred to the C═O band upon heating, which indicated that a dehydration process occurred during the volume phase transition. While, as far as we know, few previous works have demonstrated the comprehensive description of volume phase transitions and relevant complex interactions relating to poly(oligo(ethylene glycol) acrylate) (POEGA)-based or PNIPAM-based nanogels at molecular level.

The nanogels studied in this work are of core−shell architectures, which are synthesized via reversible addition−fragmentation chain transfer (RAFT) mediated aqueous dispersion polymerization. More specifically, the shells of these two nanogel systems are derived from macromolecular chain transfer agent (Macro-CTA) poly(*N*,*N*′-dimethylacrylamide) (PDMA) while the cores are composed of cross-linked poly(2-methoxyethyl acrylate-*co*-poly(ethylene glycol) methyl ether acrylate) network for the POEGA-based (P(MEA-*co*-PEGA)/PDMA) nanogels and cross-linked PNIPAM network for the PNIPAM-based (PNIPAM/PDMA) nanogels, respectively. The chemical structures of these two nanogels are illustrated in Scheme 1. As has been demonstrated by one of us

Scheme 1. Chemical Structures of P(MEA-*co*-PEGA)/PDMA (a) and PNIPAM/PDMA (b) Core−Shell Nanogels

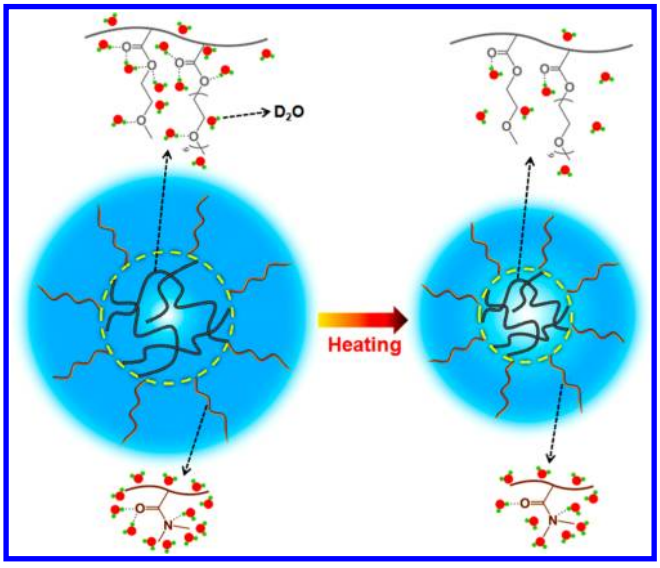

in previous works,[40,41] these two nanogels exhibit quite different thermal responsibilities: the P(MEA-*co*-PEGA)/PDMA nanogels show an unprecedented linear diameter reduction over a wide temperature range during the heating process while the PNIPAM/PDMA nanogels present a typical dramatic size decrease around VPTT upon raising temperature. Speaking of linear dependence of nanogel size vs temperature, it is relatively rare. Recently, Zeiser and co-workers[42] found that in the temperature range of 25 to 41 °C, the core−shell microgels, with a core made of poly(*N*-isopropylmethacrylamide) and a shell consisting of poly(*N*-*n*-propylacrylamide), exhibit a response of particle size directly proportional to the temperature. They attribute it to the enhanced "corset-effect" realized due to the use of two polymers with largely different LCST. Kojima et al.[43] has also discovered that PNIPAM microgels demonstrated an almost linear size reduction upon heating in mixed water/methanol solvents during a particular temperature range. However, to be best of our knowledge, the mechanism of this behavior from the view of molecular level has not yet been explored.

In this work, we try to elucidate the mechanistic differences for the different volume phase transition behavior of P(MEA-*co*-PEGA)/PDMA and PNIPAM/PDMA nanogels using FTIR in the combination with two-dimensional correlation spectroscopy (2Dcos). For the core−shell nanogels, FTIR is the technique of choice in exploring the behavior of the core and the shell during the volume phase transition as the characteristic peaks of the core and shell can be separately probed in the IR spectra. In this way, we are able to differentiate the roles of the inner core and the outer shell of the nanogels during the volume phase transition process. Furthermore, 2Dcos has also

dx.doi.org/10.1021/ma4021906 | *Macromolecules* 2014, 47, 1144−1154

been proved to be effective methods in elucidating the phase transition behavior of thermal responsive polymers including PNIPAM,[44] PVCL,[45] poly(vinyl methyl ether) (PVME),[46] and OEG(M)A-based linear polymers.[47] With the aid of 2Dcos, additional information on microscopic variations of complicated interactions in the nanogels during the volume phase transition process can be extracted, and therefore, a more comprehensive understanding of the relationship between the structure and the thermal responsive properties of the nanogels can be obtained.

2. EXPERIMENTAL SECTION

2.1. Materials. P(MEA-*co*-PEGA)/PDMA and PNIPAM/PDMA core−shell nanogels were synthesized according to previous reports.[40,41] Typically, RAFT dispersion polymerization of MEA and PEGA of 90/10 molar ratio was carried out at 70 °C in water for P(MEA-*co*-PEGA)/PDMA nanogel synthesis. Herein, PDMA was used as macro-CTA and poly(ethylene glycol diacrylate) (PEGDA) was used as cross-linker. Macro-CTA (0.106 g, 0.021 mmo), MEA (0.245 g, 1.89 mmol), and PEGA (0.099 g, 0.21 mmol) were dissolved in 4 mL of deionized water. The solution was degassed with N_2 in ice water for 40 min before immersion into a preheated oil bath at 70 °C. After the temperature was stabilized, a degassed solution of 2,2′-azobis(2-methylpropionamidine) dihydrochloride (V-50) (0.3 mg, 1.1 mmol) was injected through a syringe. The polymerization reaction was continued under the protection of N_2 for 5 h and then stopped by sudden cooling in ice water. D_2O was purchased from Cambridge Isotope Laboratories Inc. (D-99.9%). The freeze-dried nanogels were dispersed in D_2O at a fixed concentration of 10 wt % and were kept at 4 °C for a week to ensure sufficient swelling of the nanogels and complete deuteration of all the N−H protons before FTIR measurement. Then, the nanogels were fully swollen to form a relatively viscous solution.

2.2. Instruments and Measurements. The samples of nanogel D_2O solutions for FTIR measurement were prepared by sealing the dispersions between two ZnS tablets. All the time-resolved FTIR spectra at variable temperatures were recorded by using a Nicolet Nexus 6700 FTIR spectrometer equipped with a DTGS detector. 32 scans at a resolution of 4 cm^{-1} were accumulated to obtain an acceptable signal-to-noise ratio. Temperatures were under programmed control with an electronic cell holder at a rate of ca. 1 °C/3 min with an increment of 0.5 °C (accuracy: 0.1 °C). The neat P(MEA-*co*-PEGA)/PDMA and PNIPAM/PDMA nanogel films for FTIR measurement were prepared by drop-casting on the ZnS tablets from their aqueous dispersions. Baseline correction was performed by the software of OMINIC 6.1a.

The volume phase transitions of the nanogels were monitored on a dynamic light scattering (DLS)-zetasizer nanosystem (Malvern) (scattering angle: 173°) by following the reduction of the hydrodynamic diameter of nanogels upon heating with an increment of 1 °C. In order to obtain sufficient equilibration of the nanogels, each temperature was maintained constant for 5 min. The nanogels for DLS measurements were swollen in H_2O and D_2O at a concentration of 1 mg/mL.

2.3. Investigation Method. *Two-Dimensional Correlation Analysis (2Dcos).* The temperature-dependent FTIR spectra recorded at an internal of 0.5 °C in certain wavenumber ranges were selected to perform 2D correlation analysis. 2D correlation analysis was conducted using the software of 2D Shige ver. 1.3 (Shigeaki Morita, Kwansei Gakuin University, Japan, 2004−2005) and was further plotted into the contour maps by Origin Program ver. 8.0. In the contour maps, red colors are defined as positive intensities, while the green colors are defined as negative ones.

3. RESULTS AND DISCUSSION

3.1. DLS Measurements. First, DLS measurements were performed for P(MEA-*co*-PEGA)/PDMA and PNIPAM/PDMA core−shell nanogels in both H_2O and D_2O to determine the hydrodynamic diameter with increasing temperature. Figure 1 presents the temperature-induced transition

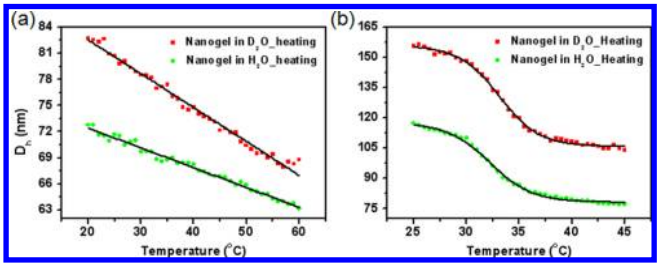

Figure 1. DLS measurements of P(MEA-*co*-PEGA)/PDMA (20−60 °C) (a) and PNIPAM/PDMA (25−45 °C) (b). The concentration of nanogels is 1.0 mg/mL.

curves measured by DLS for P(MEA-*co*-PEGA)/PDMA and PNIPAM/PDMA core−shell nanogels. As can be seen from the figures, the nanoparticle sizes in D_2O for both nanogels are relatively larger than that in H_2O, which is probably attributed to the stronger deuterium bonding of the C═O groups compared with the hydrogen bonding that occurs to water.[48,49] However, the type of solvent has little influence on the variation tendency of the volume phase transition for both systems. Herein, we will mainly focus on the volume phase transition of nanogels in D_2O solution. For P(MEA-*co*-PEGA)/PDMA nanogels, an unexpected linear decrease in diameter during the whole heating process (20−60 °C) is observed, indicating that the nanogels have a gradual hydrophilic-to-hydrophobic conformation transformation. This phenomenon is in absolute contrast to the sharp LCST transition exhibited by the corresponding linear copolymers of P(MEA-*co*-PEGA).[41] While for the PNIPAM/PDMA nanogels, an obvious volume phase transition around 33 °C is obtained, which can also be observed in the calorimetric measurements (Figure S1, Supporting Information). It is almost similar to the behavior of linear PNIPAM chains. Moreover, it should be noticed that the temperature's effect on P(MEA-*co*-PEGA)/PDMA nanogels is smaller than PNIPAM/PDMA nanogels. Similar observation has also been reported for OEGMA-based microgels synthesized via free radical precipitation copolymerization.[24] Thus, we suppose that such difference is originated from the structures of monomers, in which NIPAM has both H-donor (N−H) and H-acceptor (C═O) and the internal hydrogen-bond structure C═O···H−N contributes a lot to its phase transition behavior while OEGMA lacks of H-donor and the collapse is only driven by hydrophobic interactions. And this will be farther confirmed by the FTIR analysis in the next part. In order to find the plateau at high temperature, we have also carried out the DLS measurement in a wider temperature range (see Figure S2). It demonstrates that the plateau only begins to appear at around 70 °C, at which the polymer chains were cross-linked. In the synthesis of nanogels, only 3 mol % (relative to the total amount of monomers) cross-linkers were used in order to minimize the effect of the cross-linkers on the thermoresponsive behavior of the nanogels. However, different cross-linkers were used for these two nanogels, poly(ethylene glycol diacrylate) (M_n = 258) for P(MEA-*co*-PEGA)/PDMA nanogel and *N*,*N*′-methylenebis(acrylamide) for PNIPAM/PDMA nanogel, respectively. In order to eliminate the possible effect of cross-linker structure on the thermoresponsive behavior, we also synthesized P(MEA-*co*-PEGA)/PDMA nanogel using *N*,*N*′-methylenebis(acrylamide) as a control

dx.doi.org/10.1021/ma4021906 | *Macromolecules* 2014, 47, 1144−1154

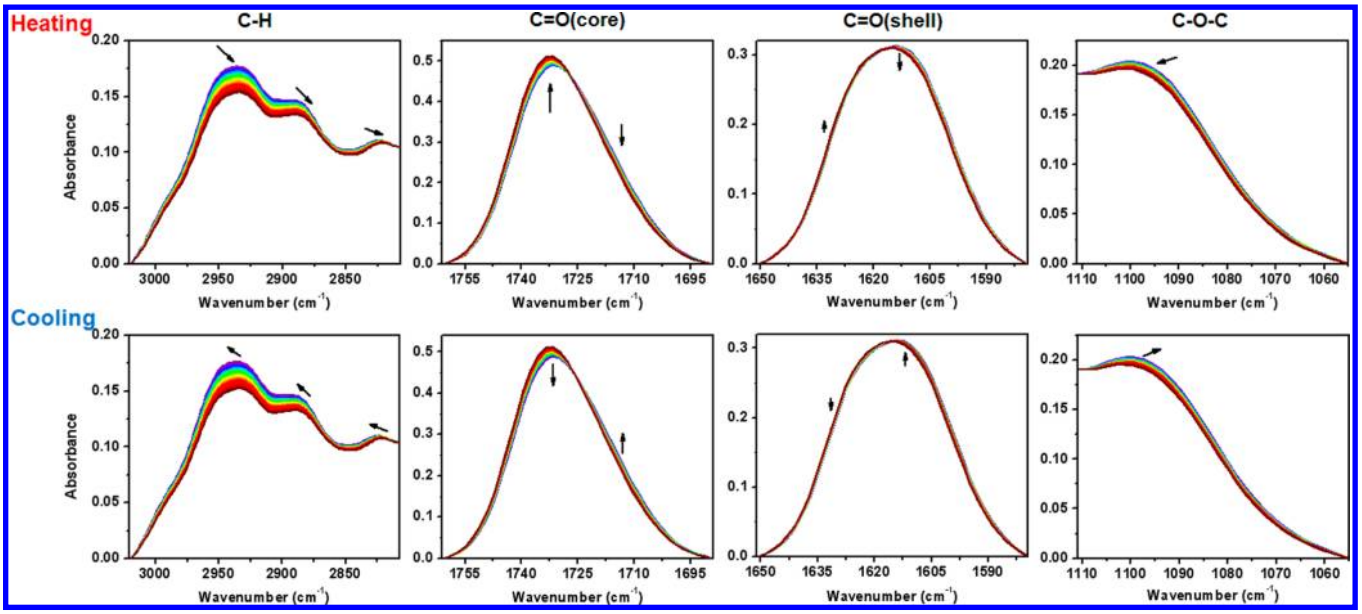

Figure 2. Temperature-dependent FTIR spectra of P(MEA-*co*-PEGA)/PDMA nanogels in D_2O (10 wt %) during heating and cooling between 25 and 41 °C with an interval of 0.5 °C in the regions 3020−2808, 1760−1690, 1650−1580, and 1110−1055 cm^{-1}.

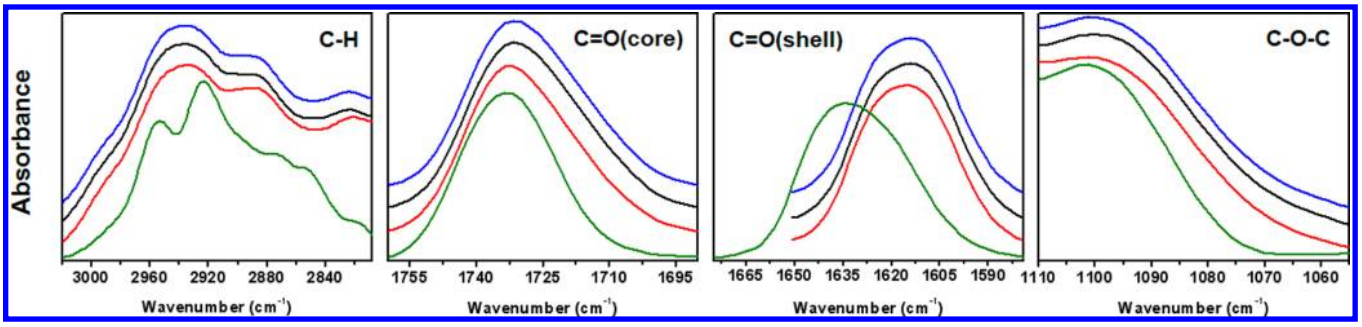

Figure 3. Spectral comparison of P(MEA-*co*-PEGA)/PDMA nanogels in D_2O (10 wt %) at 25 and 41 °C during heating and cooling and neat P(MEA-*co*-PEGA)/PDMA nanogel film (green, neat film; red, in D_2O at 41 °C; black, in D_2O at 25 °C during heating; blue, in D_2O at 25 °C during cooling).

sample (its structure scheme is illustrated in Scheme S1). This control sample also exhibited a linear response of diameter to temperature over the range of 10−60 °C (Figure S3). From these results, we can conclude that the unique linear response of P(MEA-*co*-PEGA)/PDMA nanogel is indeed derived from its inherent structure. In a previous work on the comparison of linear PNIPAM and OEGMA-based polymers,[19] the former demonstrated a relatively sharper transition than the latter one. As for the OEGMA-based nanogels prepared by other techniques,[24,27] the volume phase transitions are also rather broader than those of PNIPAM-based nanogels. Hence, we suppose that both the monomer structure and the confined network are crucial to the thermo-responsive properties of nanogels, which will be further explored in the following sections.

3.2. IR Analysis of P(MEA-*co*-PEGA)/PDMA Nanogels. *3.2.1. Conventional IR Analysis.* In IR analysis, D_2O, rather than H_2O, was selected as the solvent to eliminate the overlap of the δ(O−H) band relating to water molecule at about 1640 cm^{-1} with the ν(C═O) of nanogels as well as the broad ν(O−H) of water around 3300 cm^{-1} with ν(C−H). As shown in Figure 1, the isotopic substitutions do not affect the volume phase transition behavior of the nanogels except for slightly increasing the nanoparticle size. Therefore, it is much proper to utilize D_2O instead of H_2O for this study.

The temperature-dependent FTIR spectra of P(MEA-*co*-PEGA)/PDMA core−shell nanogels in D_2O (10 wt %) during a heating-and-cooling process between 25 and 41 °C are shown in Figure 2. Herein, we specifically focus on the following four spectral regions: C−H stretching region (3020−2808 cm^{-1}), C═O (core) stretching region (1760−1690 cm^{-1}), C═O (shell) stretching region (1650−1580 cm^{-1}), and C−O−C stretching region (1110−1055 cm^{-1}). In this way, we are able to probe almost all the group movements of the core−shell nanogels during the volume phase transition. As shown in Figure 2, for the heating process, all the C−H groups shift slightly to lower frequency on heating, indicating the changes of interactions between the hydrophobic moieties of the polymer and water molecules in the system. Considering the fact that more water molecules surrounding the C−H group leads to a higher vibrational frequency,[50] we believe that the C−H groups undergo dehydration with increasing temperature. Meanwhile, the main bands corresponding to C═O of both the core and the shell as well as those of C−O−C exhibit a blue shift, indicating the break of hydrogen bonds between oxygen atoms in the nanogel network and water. Thus, a volume phase transition of the nanogels during heating is observed in the

dx.doi.org/10.1021/ma4021906 | *Macromolecules* 2014, 47, 1144−1154

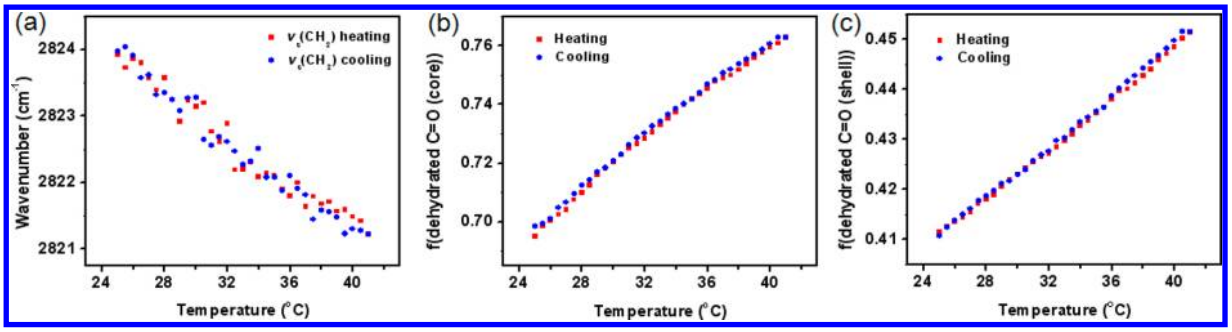

Figure 4. Temperature-dependent frequency shift of P(MEA-*co*-PEGA)/PDMA nanogels of $\nu_s(CH_2)$ (a) as well as relative content of dehydrated C═O in both the core (b) and the shell (c) during heating and cooling, respectively.

temperature-resolved FTIR spectra: together with the increase in hydrophobicity of the polymer chains, water molecules are expelled out of the nanogels at the same time. During the cooling process, the case is just opposite to that of the heating.

To further elucidate the interactions between water molecules and the polymer chains in the nanogels, some contrast FTIR curves of P(MEA-*co*-PEGA)/PDMA nanogels in D_2O at 25 and 41 °C during heating and cooling and the neat film of the nanogels are plotted in Figure 3. In the neat film, the chemical groups are believed to be free of hydrophobic hydration or hydrogen bonds with water. Compared with the neat film, the C−H, C═O, and C−O−C groups in the nanogel networks are all partially hydrated at both 25 and 41 °C, indicating that those groups in the polymer chains experience only partial dehydration with increasing temperature. This phenomenon may be explained by the fact that both the confined network topologies and the hydrophilic shell of the nanogels hinder the complete expelling of water out of the interior of the nanogels. Noteworthily, for the C═O of the core and the shell, it should be noted that the degree of hydration of the core is much lower than that of the shell, further confirming that the hydrophilic shell of the nanogel acts as a buffer between the thermally responsive core of the nanogel and the bulk water and hence plays an important role in preventing the nanogels from aggregating in the system. According to our previous experimental experience, freeze-dried nanogels without a hydrophilic shell can hardly be redispersed in water at such a high concentration of 10 wt %.

For more detailed information on temperature's influence on the hydration states of different chemical groups during the volume phase transition of the nanogels, we examined the frequency shift of $\nu_s(CH_2)$ as well as quantitative analysis of relative content of dehydrated C═O in both the core and the shell during temperature variations. As shown in Figure 4a, for P(MEA-*co*-PEGA)/PDMA nanogels, the wavenumber of $\nu_s(CH_2)$ decreases linearly upon raising temperature, demonstrating a gradual dehydration process of the CH_2 groups. This result parallels well with the DLS measurements. The thermal profile of the nanogels is totally reversible without hysteresis upon cooling. There are two different kinds of C═O groups in the nanogels, namely C═O of the amide group in the shell and C═O of the ester group in the core. By monitoring these C═O groups in the nanogels, we are able to find out the variation difference between the core and the shell during the volume phase transition. The ν(C═O) bands of the core can be divided into two Gaussian sub-bands at 1733 and 1715 cm^{-1}, in which the band at the higher wavenumber can be attributed to the (relatively) dehydrated C═O and the lower one is related to the (relatively) hydrated C═O.[51] With the assumption of 1:1 conversion between the (relatively) hydrated carbonyls and the (relatively) dehydrated ones, when the peak areas of the (relatively) dehydrated C═O around 1733 cm^{-1} are plotted against the peak areas of the component around 1715 cm^{-1}(the (relatively) hydrated C═O), the slop of the fitted line yields the ratio of the molar absorption coefficient ($\varepsilon_{1733}/\varepsilon_{1715}$) (Figure S4).[44] Figure 4b presents the temperature-dependent molar fraction of (relatively) dehydrated C═O of the core f(dehydrated C═O (core)), which is defined as $A_{1733}/[A_{1733} + A_{1715} \times (\varepsilon_{1733}/\varepsilon_{1715})]$. While for the C═O of the shell, it can be split into two sub-bands at 1626 and 1609 cm^{-1} with Gaussian curve fitting. By employing the same approach, the temperature dependence of molar fraction f(dehydrated C═O (shell)), whose definition is $A_{1626}/[A_{1626} + A_{1609} \times (\varepsilon_{1626}/\varepsilon_{1609})]$, is displayed in Figure 4c. Under this circumstance, it is more convenient to explore the changes of both the core and the shell of the nanogels during the volume phase transition. According to Figure 4b, most of the C═O groups in the core are in (relatively) dehydrated states and upon heating the molar fraction of (relatively) dehydrated C═O in the core increases linearly. With regard to C═O of the shell, based in Figure 4c, the majority of them are in the (relatively) hydrated states and the molar fraction of (relatively) dehydrated C═O in the shell also exhibits a continuous rising with heating process. The linear temperature dependence of the molar fraction of (relatively) dehydrated C═O in both the core and the shell, which is in accordance with the diameter reduction tendency, can be rooted from the gradually breaking of hydrogen bonds between the C═O groups and water molecules. The difference in the hydration states of the core and the shell is consistent with our previous discussion that the shell is more hydrophilic than the core and thus helps to stabilize the nanogels. In addition, we can directly observe that the degree of dehydration in the core is higher than that of the shell, confirming that the core dominates the volume phase transition behavior of the nanogels. The good thermal reversibility free from hysteresis of the nanogels can be further confirmed by the almost overlapping heating and cooling curves of the temperature-dependent molar fraction of the (relatively) dehydrated C═O groups.

3.2.2. Two-Dimensional Correlation Analysis. 2Dcos is a mathematics method that is originally proposed by Noda[52,53] and it has been considerably applied to interpret spectroscopic intensity fluctuations under different types of external perturbations ever since.[54] By spreading the original spectra along a second dimension, features not readily visible in conventional analysis can be sorted out and hence, spectral resolution enhancement can be achieved. In addition, 2Dcos can be applied to deduce the specific sequence order of

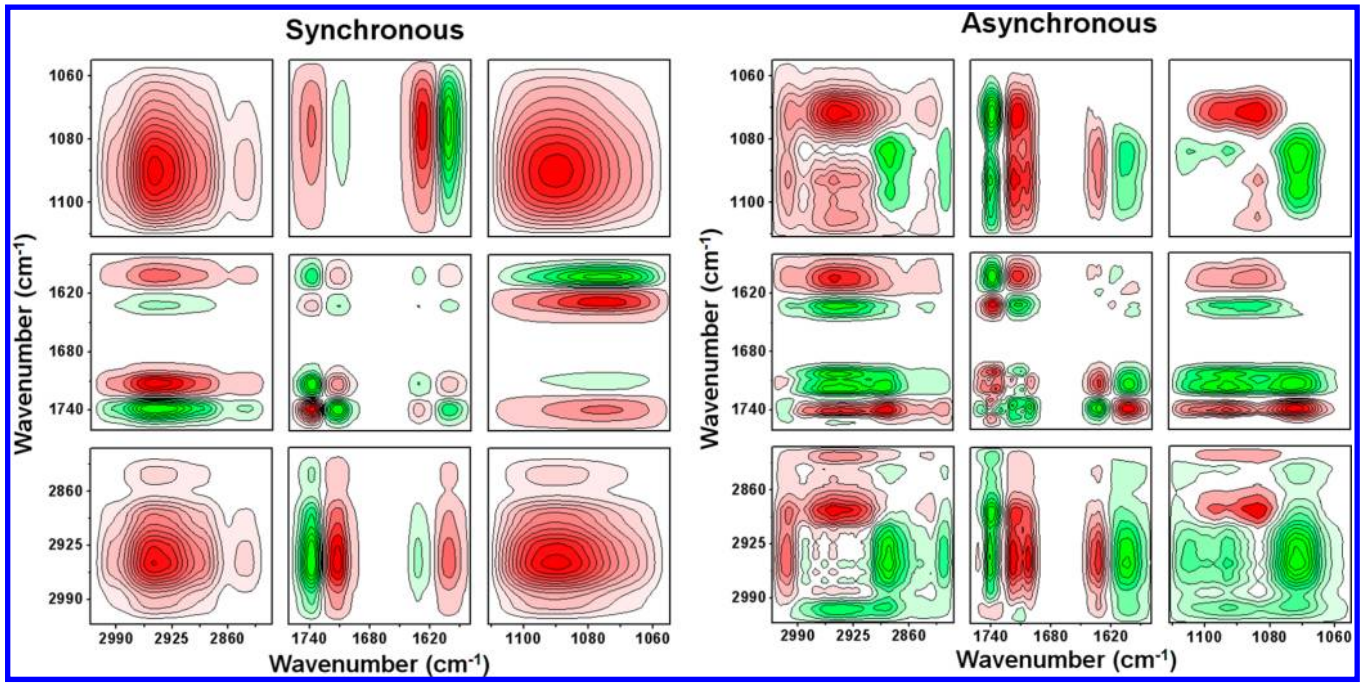

Figure 5. 2D synchronous and asynchronous spectra of P(MEA-*co*-PEGA)/PDMA nanogels in D_2O (10 wt %) during heating between 25 and 41 °C. Warm colors (red) are defined as positive intensities, while cool colors (green) are defined as negative ones.

different chemical groups under a certain physical or chemical variable.

All the FTIR spectra in heating between 25 and 41 °C with an increment of 0.5 °C are applied to generate the 2Dcos spectra and the obtained synchronous and the asynchronous spectra are shown in Figure 5. 2D synchronous spectra provide information on simultaneous changes between two wavenumbers. For instance, nearly all the bands relating to C−H and C−O−C have positive cross-peaks, indicating that they display similar sensitivities to temperature perturbation. Combined with raw spectra, it is easy to find that the intensities of all these bands decrease upon heating. Similarly, we can deduce that the intensities of the bands at 1710 and 1600 cm^{-1} decrease while those of the bands at 1736 and 1633 cm^{-1} increase in the heating process.

Two-dimensional asynchronous spectra can significantly enhance the resolution of the original spectra. As shown in Figure 5, several subtle bands such as 1749, 1741, 1719, and 1702 cm^{-1} corresponding to carbonyl groups in the nanogel core as well as C−O−C splitting bands at 1105, 1093, and 1084 cm^{-1} that cannot be determined in the 1D analysis have been identified. These additionally observed bands relating to subtle group conformations could significantly assist in figuring out the mechanism of the continuous volume phase transition of the nanogels. For clarity, all the bands detected in the asynchronous spectra and their tentative assignments are listed in Table 1. Herein, we did not distinguish the comonomers of P(MEA-*co*-PEGA) in the IR spectral assignments since they are of the same kinds (i.e., both contain a acrylate moiety and a PEG segment).[18,47]

In addition to enhancing spectral resolution, 2Dcos can also provide useful information on the specific sequence order of the chemical groups taking place under external perturbation. According to Nada's role, if cross-peaks (ν_1, ν_2) in the synchronous and asynchronous maps have the same symbol, both positive or both negative, then we can conclude that

Table 1. Tentative Band Assignments of P(MEA-*co*-PEGA)/PDMA Nanogels in D_2O According to 2Dcos Results[47,51,55]

wavenumber (cm^{-1})	tentative assignments
3001	$\nu_{as}(CH_3)(-OCH_3)$(hydrated)
2980	$\nu_{as}(CH_3)$(shell)
2970	$\nu_{as}(CH_3)(-OCH_3)$(dehydrated)
2958	$\nu_{as}(CH_2)$(backbone)
2949	$\nu_{as}(CH_2)(-OCH_2CH_2O-)$(hydrated)
2931	$\nu_{as}(CH_2)(-OCH_2CH_2O-)$(dehydrated)
2885	ν(CH)(backbone)
2835	$\nu_s(CH_2)(-OCH_2CH_2O-)$(hydrated)
2819	$\nu_s(CH_2)(-OCH_2CH_2O-)$(dehydrated)
1749	ν(C═O)(core)(dehydrated)
1741, 1736, 1719, 1710	ν(C═O)(core)(hydrating)
1702	ν(C═O)(core)(hydrated)
1639	ν(C═O)(shell)(dehydrated)
1633	ν(C═O)(shell)(hydrating)
1600	ν(C═O)(shell)(hydrated)
1105	ν(−C−O−C−)(dehydrated)
1093	ν(−C−O−C−)(hydrating)
1084	ν(−C−O−C−)(hydrated)

change at ν_1 occurs prior to that at ν_2 with the perturbation; whereas if cross-peaks (ν_1, ν_2) in the synchronous and asynchronous maps have different symbols, one positive and the other one negative, then we can infer that peak ν_2 varies prior to peak ν_1.[56] A simplified method for the determination of sequence order has been described before,[57] and here the final sequence order in the volume phase transition of the nanogels is described as (→ means earlier than or prior to) 1702 → 1719 → 3001 → 1710 → 1741 →1736 → 2970 → 1084 → 2949 → 2931 → 2958 → 1749 → 2980 → 2835 → 2885 → 1093 → 1105 →1600 → 1633 → 2819 →1639 cm^{-1} or ν(C═O)(core)(hydrated) → ν(C═O)(core)(dehydrating) → $\nu_{as}(CH_3)(-OCH_3)$(hydrated) → $\nu_{as}(CH_3)(-OCH_3)$-(dehydrated) → ν(−C−O-C−)(hydrated) → $\nu_{as}(CH_2)$-

dx.doi.org/10.1021/ma4021906 | *Macromolecules* 2014, 47, 1144−1154

(−OCH_2CH_2O−)(hydrated) → $\nu_{as}(CH_2)$(−OCH_2CH_2O−)(dehydrated) → $\nu_{as}(CH_2)$(backbone) → ν(C═O)(core)(dehydrated) → $\nu_{as}(CH_3)$(shell) → $\nu_s(CH_2)$(−OCH_2CH_2O−)(hydrated) → ν(CH)(backbone) → ν(−C−O-C−)(hydrating) → ν(−C−O-C−)(dehydrated) → ν(C═O)(shell)(hydrated) → ν(C═O)(shell)(hydrating) → $\nu_s(CH_2)$(−OCH_2CH_2O−)(dehydrated) → ν(C═O)(shell)(dehydrated).

Without considering the differences in stretching modes of the chemical groups, the specific order can be displayed as follows: C═O(core) → −$OCHH_3$(core) → −C−O−C−(core) → −$OCHH_2CH_2O$−(core) → CH_2(backbone)(core) → CH_3(shell) → CH(backbone)(core) → ν(C═O)(shell). It infers that the dehydration of hydrophobic ester groups in the core occurs first during the heating process. In this way, it is reasonable to believe that the ester groups in the network play a vital part in the volume phase transition of the nanogels. As mentioned above, there are several subtle bands emerging in the asynchronous spectra of the carbonyl groups relating to the core, indicating the existence of various dehydrating states of the C═O during the volume phase transition. It is known that C═O can form hydrogen bonds with one or two water molecules and the hydrogen bonded oxygen atom next to the C═O in the ester group may further influence the states of C═O. Thus, the diversity in the dehydrating states of the C═O here reflects the change of water environment in the nanogel core during the volume phase transition, in which the water molecules are gradually squeezed out of the interior of the nanogels, resulting in the existence of a distribution gradient of water molecules in the nanogels. To some extent, the continuous dehydrating of the C═O in the nanogel core during the heating process may contribute to the linear volume phase transition behavior of the nanogels. From the overall sequence order, we can also learn that in the nanogel core, which dominates the volume phase transition, dehydration of the pendant side chains takes place earlier than that of the backbone. This may be ascribed to the higher degree of freedom of the side chains compared to the backbone. With regard to the response of the core and the shell to the temperature, we can conclude that the conformation changes of the core occur prior to that of the shell according to the sequence order. Therefore, the volume phase transition of the P(MEA-*co*-PEGA)/PDMA nanogels upon heating can be described as follows: at lower temperatures, the nanogels are swollen by water molecules through the hydrogen bonding associated with the ester and ether groups and the hydration of the aliphatic groups. When temperature is increased, the hydrogen bonds between water molecules and the C═O in the ester groups in the core gradually break, resulting in a more hydrophobic environment at the linkage between the backbone and the pendant chains. Then the pendant ether segments start to dehydrate and collapse toward the backbone simultaneously. With increasingly hydrophobic environment in the nanogel core, the hydrophobic interactions come to dominate the volume phase transition and the nanogel core collapses along the backbone, further expelling water molecules out (Scheme 2). The hydrophilic nanogel shell responds slowly to the temperature change and it only undergoes slightly dehydration after the core. It is with the help of the PDMA shell that the aggregation of nanogels is prevented to maintain colloidal stability under heating.

3.3. IR Analysis of PNIPAM/PDMA Nanogels. *3.3.1. Conventional IR Analysis.* In order to better elucidate the mechanism of the sharp volume phase transition behavior of the PNIPAM/PDMA nanogels, we also carried out temperature-variable FTIR measurements of the nanogels in D_2O (10 wt %) during the heating-and-cooling cycle between 25 and 43 °C, as shown in Figure 6. Herein, two main spectral regions are focused on: C−H stretching region (3020−2844 cm^{-1}) and C═O stretching region (1680−1580 cm^{-1}). By monitoring these regions, details about the molecular motions of the chemical groups in the core cross-linked network during the volume phase transition can be provided.

The main spectral changes in the heating process of the nanogels can be summarized as follows: all the bands corresponding to the CH stretching present an apparent red

Scheme 2. Schematic Illustration of the Volume Phase Transition Mechanism of P(MEA-*co*-PEGA)/PDMA Core−Shell Nanogels upon Heating[a]

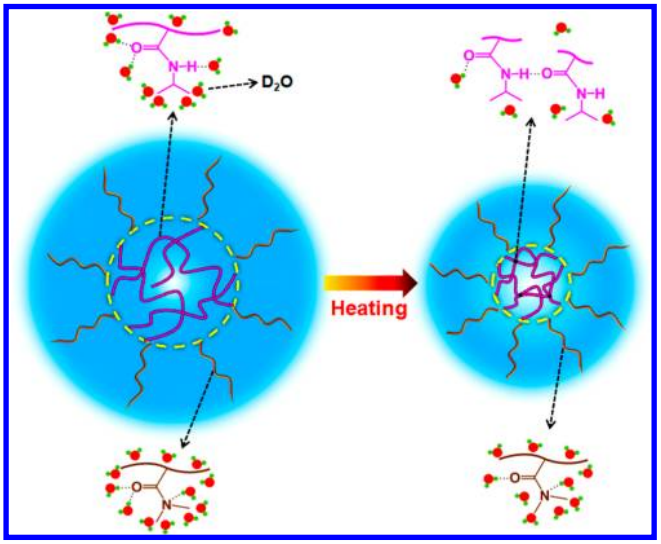

[a]The light blue color represents the distribution density of water molecules.

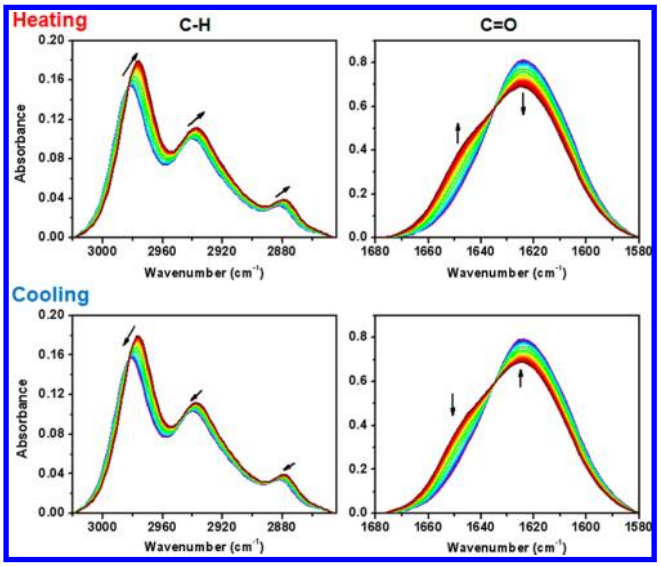

Figure 6. Temperature-dependent FTIR spectra of PNIPAM/PDMA nanogels in D_2O (10 wt %) during heating and cooling between 25 and 43 °C with the interval of 0.5 °C in the regions 3020−2844 and 1680−1580 cm^{-1}.

dx.doi.org/10.1021/ma4021906 | *Macromolecules* 2014, 47, 1144−1154

shift while in the C═O region, a bidirectional spectral intensity change is evident. Therefore, it can be deduced that with increasing temperature the hydrophobic interaction among the CH groups becomes increasingly important, thus making the CH groups undergo dehydration. As the bands located at around 1625 and 1650 cm^{-1} are assigned to the hydrogen bonds of C═O(core)···D−O−D and C═O(core)···D−N,[58,59] respectively, the spectral changes in the C═O region reveal that the chain collapse of the nanogels in the core is accompanied by the dissociation of C═O(core)···D−O−D hydrogen bonds and the formation of C═O(core)···D−N hydrogen bonds. From the primitive conventional FTIR analysis, the transition of the nanogels seems to be similar to that of the PNIPAM chains in aqueous solution except for that the nanogels exhibit a relatively less intense spectral change, which may be attributed to the confined network architecture of the nanogels. In the cooling process, the situation seems to show an opposite trend to that in the heating at a first glance.

We additionally compare the spectra of the nanogels in D_2O at 25 and 43 °C during heating and cooling and neat nanogel film to discern the effect of hydration on the frequency of the CH and C═O stretching bands, as presented in Figure 7. In

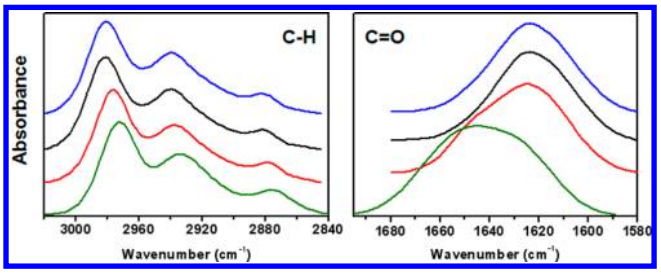

Figure 7. Spectral comparison of PNIPAM/PDMA nanogels in D_2O (10 wt %) at 25 and 43 °C during heating and cooling and neat PNIPAM/PDMA nanogel film (green, neat film; red, in D_2O at 43 °C; black, in D_2O at 25 °C during heating; blue, in D_2O at 25 °C during cooling).

the CH stretching region, all the peaks shift to lower wavenumbers after heating, indicating the dehydration of the CH groups. Meanwhile, after the volume phase transition (43 °C), the wavenumbers of the bands relating to the CH groups are still higher than that of the neat film, which means that the CH groups are still partially hydrated even after volume phase transition. This phenomenon can be also observed in the C═O stretching region. By comparing this nanogel system with linear PNIPAM in aqueous solution (Figure S5), we suppose that this incomplete dehydration behavior is originated from the existence of the hydrophilic PDMA shell, which remains in the hydration state after heating and prevents further dehydration of the core.

To quantitatively describe the volume phase transition of the nanogels, in Figure 8, we examine the temperature-dependent frequency shifts of $\nu_{as}(CH_3)$ and $\nu_{as}(CH_2)$ as well as the integral area in the region 1680−1650 cm^{-1}, which reflects the number of C═O(core)···D−N hydrogen bonds. Herein, Boltzmann fitting is performed for all the points to better understand the volume phase transition. Unlike P(MEA-*co*-PEGA)/PDMA nanogels, PNIPAM/PDMA nanogels exhibit a rather sharp transition and have an obvious VPTT at around 33 °C, which is in good accordance with the DLS measurements. It should be noted that after a heating-and-cooling cycle, both the CH and the C═O groups suffer incomplete reversibility. Taking the core−shell structure of the nanogels into consideration, once water molecules are excluded out of the nanogel core, it becomes more difficult for water molecules to go through the hydrophilic shell and diffuse into the relatively dehydrated core again. Another factor that can contribute to the irreversibility is that partial physical cross-linking through inter-/intrachain hydrogen bonds C═O(core)···D−N still remains when the temperature cools down.

3.3.2. Two-Dimensional Correlation Analysis. To further obtain the details of group motions in the volume phase transition of the PNIPAM/PDMA nanogels, all the spectra between 25 and 43 °C with an internal of 0.5 °C are used to perform the 2Dcos analysis. Figure 9 shows the 2D synchronous and asynchronous maps in the heating process of the nanogels. In the synchronous maps, the bands at 2966, 2929, 2873, and 1647 cm^{-1} all have positive cross-peaks, indicating that they have similar sensitivity of spectral intensities to the temperature perturbation; namely, all increase upon heating determined with the help of raw spectra. However, the temperature-induced intensity variations of the bands at 2991 and 1628 cm^{-1} take place in the other direction—that is, decrease on heating.

Because 2D asynchronous spectra significantly enhance spectral resolution, many subtle bands, such as the bands at 2977 and 2896 cm^{-1} corresponding to ν_{as}(dehydrating CH_3 or CH_3 in intermediate states) and ν(CH)(backbone) in the core as well as 1657 and 1600 cm^{-1} attributed to ν(dehydrated C═O) in the core and ν(hydrated C═O) in the shell, appear in the heating 2D asynchronous spectra. For the convenience of discussion, all the bands identified in asynchronous spectra and

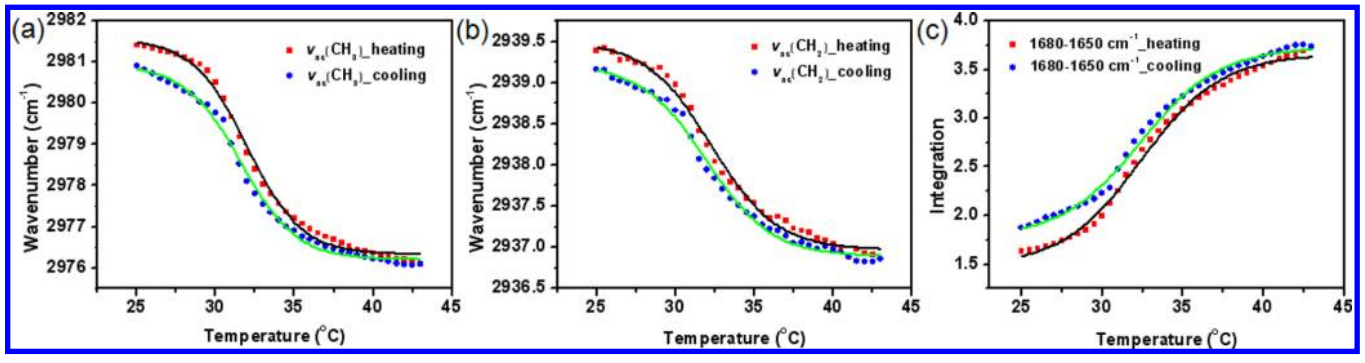

Figure 8. Temperature-dependent frequency shifts of $\nu_{as}(CH_3)$ (a) and $\nu_{as}(CH_2)$ (b) as well as the integral area in the region 1680−1650 cm^{-1} (c) during heating and cooling for PNIPAM/PDMA nanogels.

dx.doi.org/10.1021/ma4021906 | *Macromolecules* 2014, 47, 1144−1154

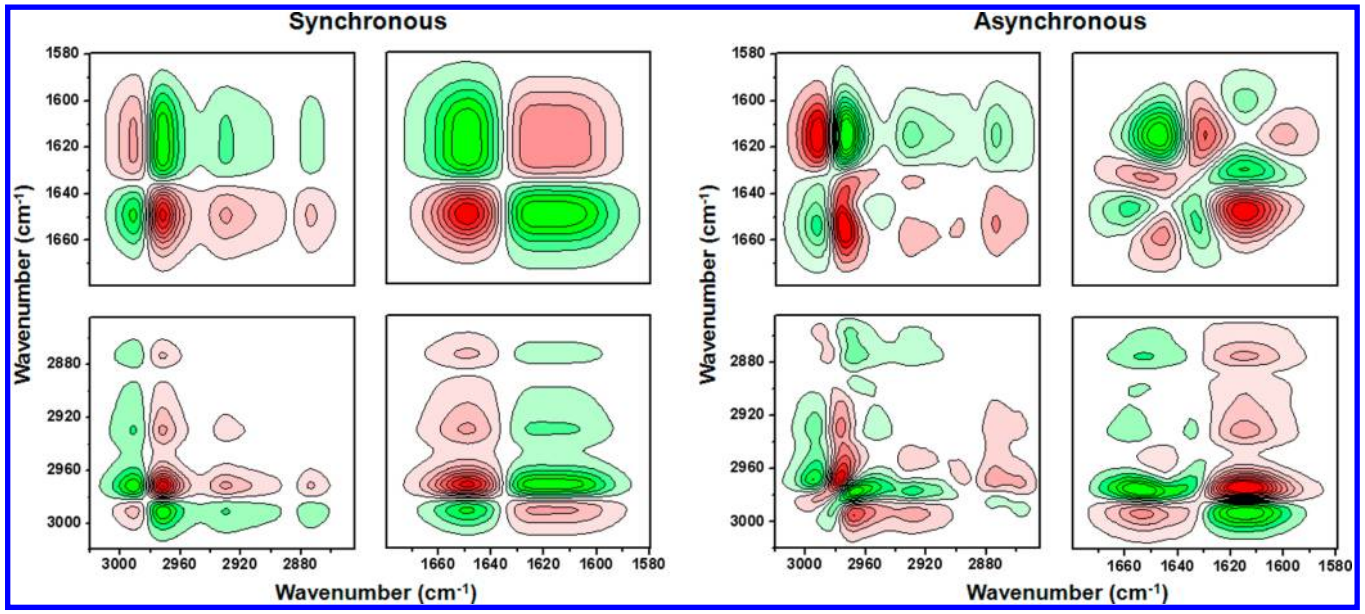

Figure 9. 2D synchronous and asynchronous spectra of PNIPAM/PDMA nanogels in D_2O (10 wt %) during heating between 25 and 43 °C. Warm colors (red) are defined as positive intensities, while cool colors (green) are defined as negative ones.

their tentative assignments during heating are summarized in Table 2.

Table 2. Tentative Band Assignments of PNIPAM/PDMA Nanogels in D_2O Based on 2Dcos Results[44,59,60]

wavenumber (cm^{-1})	tentative assignments
2991	$\nu_{as}(CH_3)$(hydrated)
2977	$\nu_{as}(CH_3)$(dehydrating)
2966	$\nu_{as}(CH_3)$(dehydrated)
2929	$\nu_{as}(CH_2)$(backbone)
2896	ν(CH)(backbone)
2873	$\nu_s(CH_3)$
1657	ν(C═O) (core)(dehydrated)
1647	ν(C═O···D−N)(core)
1628	ν(C═O)(core)(hydrated)
1600	ν(C═O)(shell)(hydrated)

Thanks to the 2D correlation analysis, the specific order of the chemical groups taking place under external perturbation can be discerned. On the basis of the Noda's rule, we can deduce the final sequence order in the heating process of the nanogels: 2991 → 2873 → 2977 → 2896 → 1628 → 2929 → 2966 → 1647 → 1600 → 1657 cm^{-1} or $\nu_{as}(CH_3)$(hydrated) → $\nu_s(CH_3)$ → $\nu_{as}(CH_3)$(dehydrating) → ν(C−H) → ν(C═O)(core)(hydrated) → $\nu_{as}(CH_2)$ → $\nu_{as}(CH_3)$(dehydrated) → ν(C═O)(C═O···D−N)(core) → ν(C═O)(shell)(hydrated) → ν(C═O)(core)(dehydrated). For the C−H groups, it shows that the pendent isopropyl groups in the nanogel core have an earlier response than the backbone in the heating process, which can be explained by the fact that the pendent groups have more conformational freedom than the backbone. Furthermore, considering only the stretching modes, it can be observed that the asymmetric stretching vibration responds earlier than the symmetric one. As reported previously, the direction of asymmetric stretching vibration is parallel to the polymer chain axis while that of symmetric stretching vibration is vertical to the polymer chain axis.[57] Thus, during the heating process, the pendent groups dehydrate first and move toward the more hydrophobic backbone and then the backbone starts to collapse, resulting in the size reduction of the nanogels. For the C═O groups, it tells that with rising temperature, the C═O···D−O−D hydrogen bonds in the core, which are more sensitive to temperature variation, break first and then the carbonyl groups are preferentially engaged in the formation of C═O···D−N hydrogen bonds, creating physical cross-links. With increasing cross-links in the nanogel core, the water content subsequently decreases, which may be responsible to the sharp change of the nanogel size. When most of the water molecules are expelled out of the nanogel core, the free C═O groups that not participating in the form of C═O···D−N or C═O···D−O−D show up. It can also be observed that, during the heating process the C═O groups in the shell change at the end of the transition, which is consistent with the fact that PDMA is not a thermal responsive material and it just functions as a stabilizer. Additionally, in the nanogel core, the faster response of the CH groups than the C═O groups may be caused by that the CH groups are relatively more hydrophobic compared with C═O groups.

On the basis of the above analysis, the molecular mechanism relating to the sharp phase transition of the PNIPAM/PDMA nanogels in the heating process can be proposed, as illustrated in Scheme 3. At temperatures below VPTT, both the CH and C═O groups in the nanogels are associated with water molecules and thus the nanogels stay in the well swollen states. As temperature increases up to VPTT, the pendent CH_3 groups in the nanogel core dehydrate first and then the backbone starts to collapse, which is driven by both the increasing hydrophobic interactions and the conversion of water-associated amide hydrogen bonds to inter-/intramolecular ones among polymer chains. Particularly, with the help of increasing inter/intramolecular hydrogen bonds, functioning as physical cross-links, water molecules can be further expelled out of the nanogel core, thus leading to the abrupt decrease of the hydrodynamic diameter of the nanogels. In the heating process, the hydrophilic nanogel shell is relatively stable and only experiences slight dehydration at the latter stage of the volume phase transition of the nanogels.

dx.doi.org/10.1021/ma4021906 | Macromolecules 2014, 47, 1144−1154

Scheme 3. Schematic Illustration of the Mechanism of the Volume Phase Transition of PNIPAM/PDMA Core−Shell Nanogels during Heating[a]

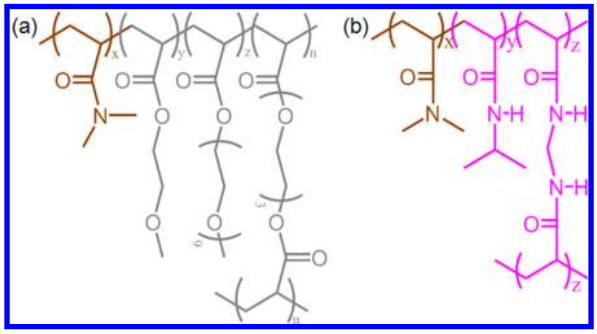

[a]The light blue color represents the distribution density of water molecules.

4. CONCLUSIONS

In this paper, we employed DLS and FTIR measurements, in combination with 2Dcos, to investigate the thermally induced volume phase transition behavior of the P(MEA-*co*-PEGA)/PDMA and PNIPAM/PDMA core−shell nanogels by in situ tracing at the molecular level. In the DLS measurements, the P(MEA-*co*-PEGA)/PDMA nanogels exhibit an unexpected linear temperature dependence of hydrodynamic diameter while the PNIPAM/PDMA nanogels display a relatively sharp volume phase transition in the heating process. Those phenomena can be also observed in the temperature-dependent FTIR spectra and corresponding quantitative analysis. On the basis of the 2D correlation analysis, we attribute the gradual dehydration of the C═O groups in the nanogel core to be the dominant effect on the linear volume phase transition behavior of P(MEA-*co*-PEGA)/PDMA nanogels and the inter/intramolecular C═O···D−N hydrogen bonds, acting as additional cross-links during the transition, to be the driving force of the sharp volume phase transition of the PNIPAM/PDMA nanogels. Moreover, from both the 1D and 2D IR analysis of those two nanogels systems, we find that thermally induced variation in the outer shell is far less significant than that in the inner core, indicating that the hydrophilic shell does function as a stabilizer, which helps the nanogels to redisperse and protects them from aggregating in the volume phase transition.

■ ASSOCIATED CONTENT

Supporting Information

Calorimetric measurements of P(MEA-*co*-PEGA)/PDMA and PNIPAM/PDMA nanogels (Figure S1), DLS data of P(MEA-*co*-PEGA)/PDMA core−shell nanogels in heating from 4 to 80 °C (Figure S2), chemical structure of P(MEA-*co*-PEGA)/PDMA nanogel using *N*,*N*′-methylenebis(acrylamide) as cross-linker (Scheme S1), DLS measurements of P(MEA-*co*-PEGA)/PDMA core−shell nanogels cross-linked with *N*,*N*′-methylenebis(acrylamide) (Figure S3), details of calculating the ratios of molar absorption coefficient of different kinds of C═O groups in the P(MEA-*co*-PEGA)/PDMA nanogels (Figure S4), temperature-dependent FTIR spectra of linear PNIPAM in D_2O (10 wt %) in heating between 25 and 43 °C (Figure S5), and PCMW spectra of P(MEA-*co*-PEGA)/PDMA (Figure S6) and PNIPAM/PDMA (Figure S7) core−shell nanogels in D_2O during heating and related discussion. This material is available free of charge via the Internet at http://pubs.acs.org.

■ AUTHOR INFORMATION

Corresponding Authors

*E-mail: peiyiwu@fudan.edu.cn (P.W.).
*E-mail: an.zesheng@shu.edu.cn (Z.A.).

Notes

The authors declare no competing financial interest.

■ ACKNOWLEDGMENTS

We are very grateful for the financial support of the National Natural Science Foundation of China (NSFC) (Nos. 20934002, 51073043, 21274084).

■ REFERENCES

(1) Saunders, B. R.; Vincent, B. *Adv. Colloid Interface Sci.* **1999**, *80*, 1−25.
(2) Pelton, R. *Adv. Colloid Interface Sci.* **2000**, *85*, 1−33.
(3) An, Z. S.; Qiu, Q.; Liu, G. Y. *Chem. Commun.* **2011**, *47*, 12424−12440.
(4) Chen, G. H.; Hoffman, A. S. *Macromol. Rapid Commun.* **1995**, *16*, 175−182.
(5) Eichenbaum, G. M.; Kiser, P. F.; Dobrynin, A. V.; Simon, S. A.; Needham, D. *Macromolecules* **1999**, *32*, 4867−4878.
(6) Lu, X.; Sun, M.; Barron, A. E. *J. Colloid Interface Sci.* **2011**, *357*, 345−353.
(7) Bergbreiter, D. E.; Case, B. L.; Liu, Y. S.; Caraway, J. W. *Macromolecules* **1998**, *31*, 6053−6062.
(8) Lu, Y.; Yuan, J.; Polzer, F.; Drechsler, M.; Preussners, J. *ACS Nano* **2010**, *4*, 7078−7086.
(9) Reese, C. E.; Mikhonin, A. V.; Kamenjicki, M.; Tikhonov, A.; Asher, S. A. *J. Am. Chem. Soc.* **2004**, *126*, 1493−1496.
(10) Zhu, H.; Li, Y.; Qiu, R.; Shi, L.; Wu, W.; Zhou, S. *Biomaterials* **2012**, *33*, 3058−3069.
(11) Wu, W.; Zhou, T.; Berliner, A.; Banerjee, P.; Zhou, S. *Chem. Mater.* **2010**, *22*, 1966−1976.
(12) Alvarez-Puebla, R. A.; Contreras-Caceres, R.; Pastoriza-Santos, I.; Perez-Juste, J.; Liz-Marzan, L. M. *Angew. Chem., Int. Ed.* **2009**, *48*, 138−143.
(13) Wu, W.; Mitra, N.; Yan, E. C. Y.; Zhou, S. *ACS Nano* **2010**, *4*, 4831−4839.
(14) Zhang, J. G.; Xu, S. Q.; Kumacheva, E. *J. Am. Chem. Soc.* **2004**, *126*, 7908−7914.
(15) Wei, H.; Cheng, S.-X.; Zhang, X.-Z.; Zhuo, R.-X. *Prog. Polym. Sci.* **2009**, *34*, 893−910.
(16) Lutz, J. F.; Hoth, A. *Macromolecules* **2006**, *39*, 893−896.
(17) Hu, Z.; Cai, T.; Chi, C. *Soft Matter* **2010**, *6*, 2115−2123.
(18) Lutz, J.-F. *J. Polym. Sci., Part A: Polym. Chem.* **2008**, *46*, 3459−3470.
(19) Lutz, J.-F.; Akdemir, O.; Hoth, A. *J. Am. Chem. Soc.* **2006**, *128*, 13046−13047.
(20) Wischerhoff, E.; Uhlig, K.; Lankenau, A.; Boerner, H. G.; Laschewsky, A.; Duschl, C.; Lutz, J.-F. *Angew. Chem., Int. Ed.* **2008**, *47*, 5666−5668.
(21) Lutz, J.-F. *Adv. Mater.* **2011**, *23*, 2237−2243.
(22) Weber, C.; Hoogenboom, R.; Schubert, U. S. *Prog. Polym. Sci.* **2012**, *37*, 686−714.
(23) Shen, W.; Chang, Y.; Liu, G.; Wang, H.; Cao, A.; An, Z. *Macromolecules* **2011**, *44*, 2524−2530.
(24) Cai, T.; Marquez, M.; Hu, Z. *Langmuir* **2007**, *23*, 8663−8666.
(25) Dong, H.; Mantha, V.; Matyjaszewski, K. *Chem. Mater.* **2009**, *21*, 3965−3972.
(26) Chi, C.; Cai, T.; Hu, Z. *Langmuir* **2009**, *25*, 3814−3819.
(27) Dong, H.; Matyjaszewski, K. *Macromolecules* **2010**, *43*, 4623−4628.
(28) Zhou, T.; Wu, W.; Zhou, S. *Polymer* **2010**, *51*, 3926−3933.
(29) Varga, I.; Gilanyi, T.; Meszaros, R.; Filipcsei, G.; Zrinyi, M. *J. Phys. Chem. B* **2001**, *105*, 9071−9076.

(30) Wu, X.; Pelton, R. H.; Hamielec, A. E.; Woods, D. R.; McPhee, W. *Colloid Polym. Sci.* **1994**, *272*, 467−477.
(31) Stieger, M.; Richtering, W.; Pedersen, J. S.; Lindner, P. *J. Chem. Phys.* **2004**, *120*, 6197−6206.
(32) Kratz, K.; Hellweg, T.; Eimer, W. *Polymer* **2001**, *42*, 6631−6639.
(33) Mason, T. G.; Lin, M. Y. *Phys. Rev. E* **2005**, *71*, 040801−4.
(34) Guillermo, A.; Addad, J. P. C.; Bazile, J. P.; Duracher, D.; Elaissari, A.; Pichot, C. *J. Polym. Sci. Pt. B-Polym. Phys.* **2000**, *38*, 889−898.
(35) Hofmann, C. H.; Plamper, F. A.; Scherzinger, C.; Hietala, S.; Richtering, W. *Macromolecules* **2013**, *46*, 523−532.
(36) Balaceanu, A.; Verkh, Y.; Demco, D. E.; Moeller, M.; Pich, A. *Macromolecules* **2013**, *46*, 4882−4891.
(37) Keerl, M.; Smirnovas, V.; Winter, R.; Richtering, W. *Angew. Chem., Int. Ed.* **2008**, *47*, 338−341.
(38) Keerl, M.; Smirnovas, V.; Winter, R.; Richtering, W. *Macromolecules* **2008**, *41*, 6830−6836.
(39) Liu, T.; Chen, J.; Sugihara, S.; Maeda, Y. *Colloid Polym. Sci.* **2012**, *290*, 763−767.
(40) An, Z.; Shi, Q.; Tang, W.; Tsung, C.-K.; Hawker, C. J.; Stucky, G. D. *J. Am. Chem. Soc.* **2007**, *129*, 14493−14499.
(41) Liu, G.; Qiu, Q.; An, Z. *Polym. Chem.* **2012**, *3*, 504−513.
(42) Zeiser, M.; Freudensprung, I.; Hellweg, T. *Polymer* **2012**, *53*, 6096−6101.
(43) Kojima, H.; Tanaka, F.; Scherzinger, C.; Richtering, W. *J. Polym. Sci., Part B: Polym. Phys.* **2013**, *51*, 1100−1111.
(44) Sun, B.; Lin, Y.; Wu, P.; Siesler, H. W. *Macromolecules* **2008**, *41*, 1512−1520.
(45) Sun, S.; Wu, P. *J. Phys. Chem. B* **2011**, *115*, 11609−11618.
(46) Sun, B.; Lai, H.; Wu, P. *J. Phys. Chem. B* **2011**, *115*, 1335−1346.
(47) Sun, S.; Wu, P. *Macromolecules* **2013**, *46*, 236−246.
(48) Pinkrah, V. T.; Beezer, A. E.; Chowdhry, B. Z.; Gracia, L. H.; Mitchell, J. C.; Snowden, M. J. *Langmuir* **2004**, *20*, 8531−8536.
(49) Saunders, B. R.; Crowther, H. M.; Morris, G. E.; Mears, S. J.; Cosgrove, T.; Vincent, B. *Colloid Surf. A-Physicochem. Eng. Asp.* **1999**, *149*, 57−64.
(50) Schmidt, P.; Dybal, J.; Trchova, M. *Vibr. Spectrosc.* **2006**, *42*, 278−283.
(51) Maeda, Y.; Kubota, T.; Yamauchi, H. *Langmuir* **2007**, *23*, 11259−11265.
(52) Noda, I. *Appl. Spectrosc.* **1993**, *47*, 1329−1336.
(53) Noda, I.; Dowrey, A. E.; Marcott, C.; Story, G. M.; Ozaki, Y. *Appl. Spectrosc.* **2000**, *54*, 236A−248A.
(54) Noda, I. *J. Mol. Struct.* **2008**, *883*, 2−26.
(55) Maeda, Y.; Yamauchi, H.; Kubota, T. *Langmuir* **2009**, *25*, 479−482.
(56) Noda, I. *Appl. Spectrosc.* **2000**, *54*, 994−999.
(57) Sun, S.; Tang, H.; Wu, P.; Wan, X. *Phys. Chem. Chem. Phys.* **2009**, *11*, 9861−9870.
(58) Cheng, H.; Shen, L.; Wu, C. *Macromolecules* **2006**, *39*, 2325−2329.
(59) Maeda, Y.; Higuchi, T.; Ikeda, I. *Langmuir* **2000**, *16*, 7503−7509.
(60) Sun, S.; Hu, J.; Tang, H.; Wu, P. *J. Phys. Chem. B* **2010**, *114*, 9761−9770.